JOURNAL OF MATERIALS SCIENCE 13 (1978) 1282–1290

A simple method of constructing an Ashby-type deformation mechanism map

TERENCE G. LANGDON, FARGHALLI A. MOHAMED
Department of Materials Science, University of Southern California, Los Angeles, California 90007, USA

An Ashby-type deformation mechanism map may be considerably simplified by plotting in the form of normalized stress versus the reciprocal of the homologous temperature. In this form, the boundaries separating the various fields appear as straight lines and the constant strain rate contours may be approximated as straight lines. Representative maps are presented for conditions of high temperature creep, and a simple procedure is outlined for constructing several maps for the same material at different grain sizes.

1. Introduction

It has been recognized for many years that a polycrystalline material, when subjected to an applied stress, may deform by one or more of a number of different mechanisms. An important concern in studies of mechanical behaviour is thus to identify the dominant deformation process under any selected conditions of stress, temperature, and grain size.

It was first suggested by Weertman and Weertman [1, 2] that it may be possible to construct a *creep diagram* in which the normalized stress, σ/G, is plotted as a function of the homologous temperature, T/T_m, where σ is the applied stress, G is the shear modulus, T is the absolute temperature, and T_m is the melting point of the material in degrees Kelvin. In this form, it was demonstrated schematically that the diagram may be divided into four distinct regions: Nabarro–Herring creep at very high temperatures, high temperature (Andrade) creep and low temperature (logarithmic) creep at $\sigma/G > 10^{-5}$, and anelastic (recoverable) creep at $\sigma/G < 10^{-5}$. A diagram of this type, which plots two of the variables in the basic rate equation when the other variables remain constant, is now generally referred to as a *deformation mechanism map.*

The concept of deformation mechanism mapping was first developed for real materials in the detailed work of Ashby [3] in which the best available source data were used to construct individual maps of normalized stress versus homologous temperature for several different metals and ceramics. Since this early work, similar maps have been presented for a large number of materials [4–28], and such maps are now becoming an accepted feature of materials texts [29–37].

An inherent problem with the Ashby-type map is the difficulty of construction, since a map may only be developed for a specific material by using a computer to solve the relevant constitutive equations for all the possible deformation processes at a very large number of points (typically, ~4000 to 6000) in stress–temperature space. Furthermore, having constructed a map for a material having a selected grain size, there is no simple procedure to obtain a new map for the same material with a different grain size. As a result, it is not easy to utilize directly deformation mapping techniques in practical situations.

One method of circumventing this difficulty is to plot a map using two other variables: for example, normalized grain size, $d/\mathbf{b}$, versus normalized stress, σ/G, at constant temperature, where d is the grain size and $\mathbf{b}$ is the Burgers vector [38, 39], or normalized grain size, $d/\mathbf{b}$, versus the reciprocal of homologous temperature, T_m/T, at constant normalized stress [40, 41]. However, there are many situations in which it is especially attractive to display mechanical data in the form of stress versus temperature at constant grain size,

as, for example, in engineering situations where a material of a single grain size is subjected to a wide range of stresses and temperatures. The purpose of this paper is to re-examine the Ashby-type deformation mechanism map and to present a simple construction procedure which eliminates the requirement for detailed computation.

2. The Ashby-type deformation mechanism map

A schematic illustration of an Ashby-type deformation mechanism map is shown in Fig. 1, where σ/G covers eight orders of magnitude (from 10^{-8} to 1.0), the homologous temperature scale extends from absolute zero to the melting point, and the map relates to a constant value of the grain size. The thick lines on the map represent the boundaries between fields in stress–temperature space within which a single mechanism dominates the deformation behaviour. These lines therefore trace out the loci of all points where the two adjacent processes have equal strain rates; where three lines meet, the three adjacent processes make equal contributions.

The upper horizontal line, at $\sigma/G \simeq 4 \times 10^{-2}$, represents the ideal strength of the material. The field marked dislocation glide, in the normalized stress range of $4 \times 10^{3} < \sigma/G < 4 \times 10^{-2}$, corresponds to the stress–temperature regime in which the material deforms by the conservative motion

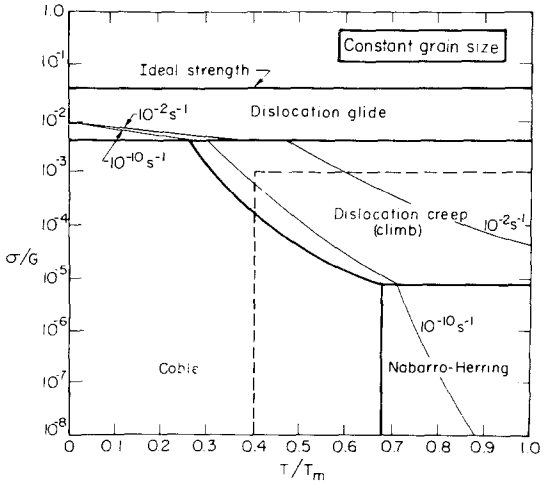

Figure 1 A schematic Ashby-type deformation mechanism map, plotting logarithmic normalized stress, σ/G, versus homologous temperature, T/T_m, for a constant grain size.

of dislocations by glide through the lattice. At values of σ/G less than $\sim 4 \times 10^{-3}$, the deformation behaviour arises from diffusion-controlled creep processes. The material deforms by a dislocation climb process at high stresses and temperatures, by Nabarro–Herring diffusional creep [42, 43] at low stresses and high temperatures, and by Coble diffusional creep [44] over the entire stress range at low temperatures.

The two thin lines superimposed on to the fields are contours of constant strain rate, for steady-state rates of 10^{-2} and 10^{-10} sec^{-1}, respectively. These lines join points in stress–temperature space having the same predicted strain rates.

Although schematic in form, Fig. 1 is identical to the maps originally developed by Ashby [3], with the exception that in some early work the strain rate contour for 10^{-8} sec^{-1} was drawn as an additional boundary to distinguish an elastic regime at lower stresses. This is justified when using a testing machine which cannot detect strain rates below 10^{-8} sec^{-1}, but in general it is usually more convenient to show the entire map and then to superimpose a number of different strain rate contours.

Without exception, all of the practical interest in the use of deformation mechanism maps has centred on their application in the analysis of data obtained from high temperature creep experiments. This interest arises because of the numerous processes which may contribute to steady-state flow under creep conditions, so that the use of maps is particularly attractive for mechanism identification. Accordingly, this paper is specifically concerned with the construction of maps for temperatures in the range from 0.4 to 1.0 T_m and for normalized stresses below 10^{-3}*: this area is indicated by the broken lines in Fig. 1.

3. Constitutive relationships for plastic flow

For the purposes of illustration, maps will be developed for high purity aluminium. This metal was selected because of the excellent experimental data available for high temperature creep, and because the same material was used for illustrative purposes in two earlier analyses [38, 40].

Four different creep mechanisms are considered: Nabarro–Herring [42, 43] and Coble [44] dif-

*A breakdown in creep behaviour generally occurs at stress levels greater than $\sim 2 \times 10^{-3}$, and the creep rate then increases essentially exponentially with stress. This breakdown is not included in Fig. 1.

fusional creep, Harper–Dorn creep [45], and a dislocation climb process. Each of these mechanisms may be represented by a constitutive relationship for the steady-state creep rate, $\dot{\epsilon}$, of the form

$$\dot{\epsilon} = AD_0 \exp(-Q/RT) \frac{Gb}{kT} \left(\frac{b}{d}\right)^p \left(\frac{\sigma}{G}\right)^n \quad (1)$$

where A is a dimensionless constant, D_0 is a frequency factor, Q is the activation energy, R is the gas constant (8.31 J mol^{-1} K^{-1} if Q is in J mol^{-1}), k is Boltzmann's constant, and p and n are constants.

The relationships for these four processes are shown in Table I, where the subscripts NH, Co, HD, and c relate to the Nabarro–Herring, Coble, Harper–Dorn, and disclocation climb processes, respectively, the subscripts l and gb refer to lattice and grain boundary diffusion, respectively, and n_c is the stress exponent for the climb process. The form of these four relationships was discussed earlier [38]. The following values were assigned to the various constants in Equations 2 to 5:

$$A_{NH} = 28,$$
$$A_{Co} = 66.8,$$
$$A_{HD} = 1.67 \times 10^{-11},$$
$$A_c = 2.5 \times 10^6,$$
$$D_{0(gb)} = D_{0(l)} = 1.86,$$
$$Q_l = 143.4 \text{ kJ mol}^{-1},$$
$$Q_{gb} = 0.6\, Q_l,$$
$$b = 2.86 \times 10^{-8} \text{ cm},$$
$$n_c = 4.4.$$

The shear modulus was taken as $G = G_0 - (\Delta G)T$, where $G_0 = 3.022 \times 10^4$ MPa and $\Delta G = 16.0$ MPa K^{-1}.

The four mechanisms listed in Table I operate independently, so that the total strain rate is equal to the sum of the rates due to the four individual processes.

4. Construction of a deformation mechanism map

The problem associated with the construction of Fig. 1 is that both the field boundaries and the strain rate contours appear as curved lines, so that each map, for any selected material and grain size, must be constructed individually by computer.

The computer subroutine has been published by Frost and Ashby [12]. Briefly, it involves using the various constitutive relationships to evaluate incrementally the rate-controlling process at each of the 4000 points defined by 50 equal increments of temperature and 80 logarithmically spaced increments of stress. The position of a particular strain rate contour is obtained by searching through the stress increments at constant temperature until two adjacent increments are located which yield, respectively, strain rates lower and higher than the required value. In a similar manner, the field boundaries are obtained by locating adjacent stress increments where there is a change in the dominant mechanism. The complexity of this procedure arises in part because of the necessity of considering dislocation climb and glide as alternative mechanisms, and then choosing the faster of these two processes.

Maps of the type shown in Fig. 1 may be considerably simplified by plotting the data in the form of normalized stress, σ/G, versus the reciprocal of the homologous temperature, T_m/T. An example is shown in Fig. 2 for pure aluminium having a grain size of 100 μm, using the relationships given in Table I. Fig. 2 covers temperatures from 0.4 to 1.0 T_m and values of σ/G from 10^{-8} to 10^{-3}, so that it directly corresponds to the area contained within the broken lines in Fig. 1. As indicated in Fig. 2, a reciprocal temperature relationship leads to a map in which the boundaries separating the various fields appear as straight, rather than curved, lines.

TABLE I Constitutive relationships for deformation mechanisms in high purity aluminium

Mechanism	Constitutive relationship for $\dot{\epsilon}$ (sec^{-1})	
Nabarro–Herring	$\dot{\epsilon}_{NH} = A_{NH} D_{0(l)} \exp(-Q_l/RT) \frac{Gb}{kT}\left(\frac{b}{d}\right)^2 \left(\frac{\sigma}{G}\right)$	(2)
Coble	$\dot{\epsilon}_{Co} = A_{Co} D_{0(gb)} \exp(-Q_{gb}/RT) \frac{Gb}{kT}\left(\frac{b}{d}\right)^3 \left(\frac{\sigma}{G}\right)$	(3)
Harper–Dorn	$\dot{\epsilon}_{HD} = A_{HD} D_{0(l)} \exp(-Q_l/RT) \frac{Gb}{kT}\left(\frac{\sigma}{G}\right)$	(4)
Climb	$\dot{\epsilon}_c = A_c D_{0(l)} \exp(-Q_l/RT) \frac{Gb}{kT}\left(\frac{\sigma}{G}\right)^{n_c}$	(5)

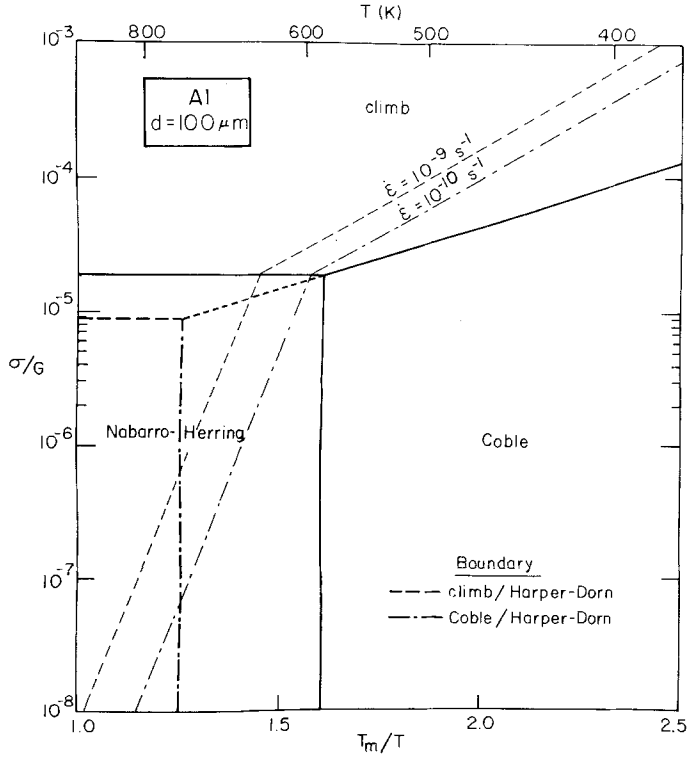

Figure 2 Deformation mechanism map of normalized stress versus the reciprocal of homologous temperature for polycrystalline aluminium having a grain size of 100 μm, covering conditions of high temperature creep ($\sigma/G \leqslant 10^{-3}$ and $T \geqslant 0.4\ T_m$).

Fig. 2 shows three different fields: dislocation climb at high stress levels, Nabarro–Herring creep at low stresses and high temperatures, and Coble creep at low stresses and low temperatures. Harper–Dorn creep does not appear on this map, because there is no value of stress and temperature at which $\dot{\epsilon}_{HD}$ is the fastest process. As indicated by the broken lines in Fig. 2, the climb/Harper–Dorn and Coble/Harper–Dorn boundaries both lie within the field for Nabarro–Herring creep, so that, for $d = 100\,\mu m$, $\dot{\epsilon}_{NH} > \dot{\epsilon}_{HD}$ under all experimental conditions.

Fig. 2 also shows two contours of constant strain rate, for $10^{-9}\ sec^{-1}$ (~ 0.01%/day) and $10^{-10}\ sec^{-1}$ (~ 3%/10 year), corresponding to a lower limiting laboratory strain rate and an upper limit for structural design purposes, respectively.

The precise method of constructing a map of this type is illustrated in Fig. 3, where the table inset summarizes the appropriate values used for the dimensionless constants, the activation energies, and the stress exponent, n_c. The procedure follows four basic steps:

(1) Since Nabarro–Herring creep and the climb process both depend on temperature through the magnitude of $\exp(-Q_1/RT)$, the boundary separating these two processes is independent of temperature. From Equations 2 and 5, the boundary is given by

$$\frac{\sigma}{G} = \left[\frac{A_{NH}}{A_c}\left(\frac{b}{d}\right)^2\right]^{1/(n_c-1)} \tag{6}$$

The corresponding relationship for the climb/Harper–Dorn boundary, obtained from Equations 4 and 5, is

$$\frac{\sigma}{G} = \left[\frac{A_{HD}}{A_c}\right]^{1/(n_c-1)} \tag{7}$$

The appearance of Harper–Dorn creep on a deformation mechanism map thus requires that the value of σ/G predicted by Equation 7 is larger than the value predicted by Equation 6. This may be expressed explicitly in the form of a required minimum grain size for Harper–Dorn creep:

$$d \geqslant b\left(\frac{A_{NH}}{A_{HD}}\right)^{1/2} \tag{8}$$

(2) Since Nabarro-Herring and Coble creep are both Newtonian viscous processes (i.e., $n = 1$), the boundary separating these two processes is independent of stress. From Equations 2 and 3, the boundary is given by

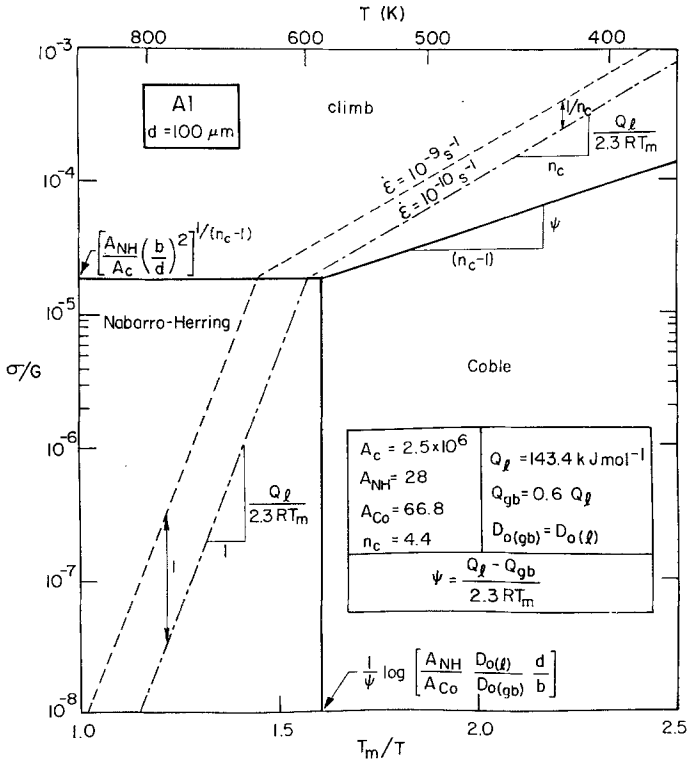

Figure 3 Method of constructing a deformation mechanism map of normalized stress versus the reciprocal of homologous temperature for conditions of high temperature creep ($\sigma/G \leqslant 10^{-3}$ and $T \geqslant 0.4\ T_m$).

$$\frac{T_m}{T} = \frac{1}{\psi}\log\left[\frac{A_{NH}}{A_{Co}}\frac{D_{o(l)}}{D_{o(gb)}}\frac{d}{b}\right] \quad (9)$$

where ψ is a constant defined as

$$\psi = \frac{Q_l - Q_{gb}}{2.3\,RT_m} \quad (10)$$

The corresponding relationship for the Coble/Harper–Dorn boundary, obtained from Equations 3 and 4, is

$$\frac{T_m}{T} = \frac{1}{\psi}\log\left[\frac{A_{HD}}{A_{Co}}\frac{D_{o(l)}}{D_{o(gb)}}\left(\frac{d}{b}\right)^3\right] \quad (11)$$

(3) On a plot of logarithmic σ/G versus T_m/T, the slope of a boundary between two adjacent mechanisms may be expressed as:

$$\text{Slope} = \frac{\Delta Q/2.3\,RT_m}{\Delta n} \quad (12)$$

where ΔQ and Δn are the differences in the activation energies and the stress exponents, respectively, for the two mechanisms on either side of the boundary. Thus, the slope of the Coble/climb boundary is equal to $\psi/(n_c - 1)$, and a line having this slope is drawn from the point of intersection of the two boundaries established by Equations 6 and 9.

(4) A contour of constant strain rate is inserted on to the map by solving one of the constitutive relationships for a selected strain rate at a point within an established field, and then drawing a straight line through this point within the field with a slope given by:

$$\text{Slope} \simeq \frac{Q/2.3\,RT_m}{n} \quad (13)$$

where Q and n apply to the appropriate mechanism in the field. Equation 13 gives slopes of $Q_l/2.3\,RT_m$ and $Q_l/2.3\,n_cRT_m$ for the Nabarro–Herring and climb fields, respectively.

Additional contours may be added to the map for different strain rates since an order of magnitude increase in $\dot{e}$ displaces the contour to higher stresses by a factor of $1/n$ when measured parallel to the normalized stress axis. Thus, strain rates which differ by an order of magnitude are separated by one order of magnitude on the σ/G scale within the Nabarro–Herring, Coble and Harper–Dorn fields.

Strictly, the drawing of straight lines within each field is not entirely correct. As indicated by the approximation in Equation 13, the relationship has been simplified by neglecting the factor G/T which occurs as a pre-exponential term in each of

the four constitutive relationships given by Equations 2 to 5. In practice, this approximation introduces only a small error which is of minor significance in comparison with the uncertainties associated with the various terms in the constitutive equations used to construct the map.*

A second error arises because the strain rates due to the different mechanisms are additive, so that the contours are slightly curved in the vicinity of the field boundaries. Again, the simplification of drawing straight lines up to the boundaries leads to an error which is very much less than the uncertainties in the constitutive relationships. This second approximation was also used by Ashby [3] in constructing the original deformation mechanism maps.

5. Construction of maps for different grain sizes

Harper–Dorn creep is not included in the map for aluminium at $d = 100\,\mu m$ because $\dot{\epsilon}_{NH} > \dot{\epsilon}_{HD}$ under all experimental conditions. The limiting grain size at which Harper–Dorn and Nabarro–Herring creep contribute equally to the observed creep rate may be obtained from Equation 8, giving $d = 370\,\mu m$.

The map for this critical grain size is shown in Fig. 4, indicating the equal contributions arising from the Harper–Dorn and Nabarro–Herring processes. At higher values of d, the Coble/Harper–Dorn boundary moves to lower temperatures, but the climb/Harper–Dorn boundary remains fixed in position because both processes are independent of grain size. Thus, the intercept on the left hand axis at $\sigma/G \simeq 9 \times 10^{-6}$ represents a lower limiting normalized stress for the transition to Newtonian viscous flow. As indicated in Fig. 5 for $d = 0.1$ cm, the Nabarro-Herring process is excluded when the climb/Nabarro–Herring and Coble/Nabarro–Herring boundaries both fall within the Harper–Dorn field.

Reference to Figs. 2 to 5 indicates that, since the climb process does not depend on grain size, the strain rate contours remain fixed in position

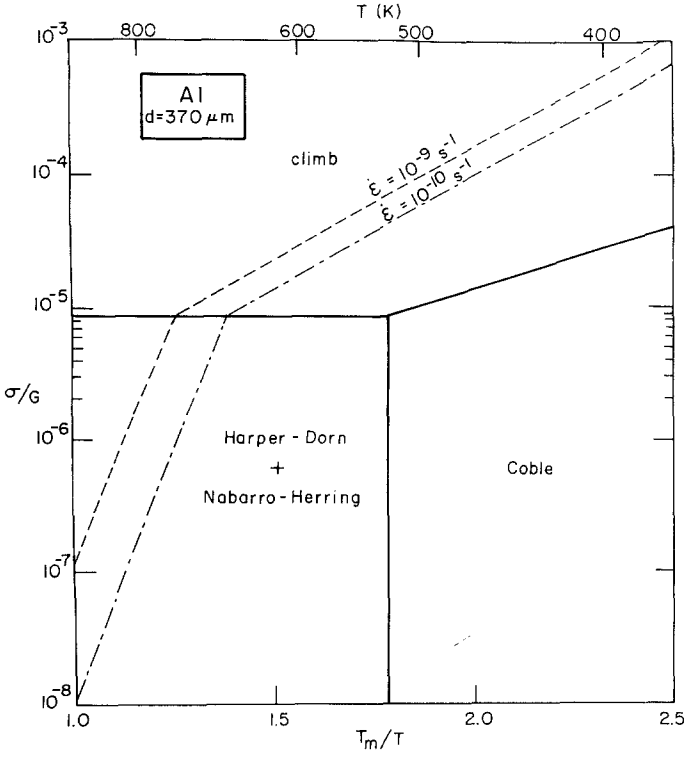

Figure 4 Deformation mechanism map of normalized stress versus the reciprocal of homologous temperature for polycrystalline aluminium having a grain size of 370 μm.

*Using the general relationship for $\dot{\epsilon}$ given in Equation 1, the variation of logarithmic σ/G with T_m/T is precisely expressed as

$$n \log\left(\frac{\sigma}{G}\right) = \log\left[\frac{\dot{\epsilon} k T}{A D_0 G b}\left(\frac{d}{b}\right)^p\right] + \frac{Q}{2.3 R T_m}\left(\frac{T_m}{T}\right) \quad (14)$$

Equation 13 neglects the slight temperature dependence resulting from the logarithmic term on the right hand side of the equality in Equation 14.

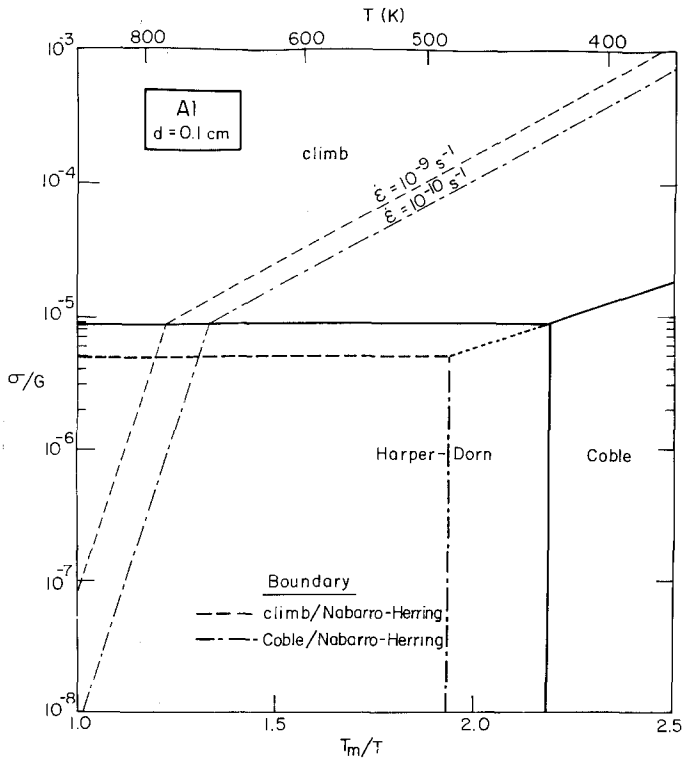

Figure 5 Deformation mechanism map of normalized stress versus the reciprocal of homologous temperature for polycrystalline aluminium having a grain size of 1.0 cm.

within the climb field. Similarly, at large grain sizes when Harper–Dorn creep becomes important, the contours also remain fixed in position within the Harper–Dorn field.* This is an attractive feature of maps of this type, since, by using Equation 13, it provides a method for plotting contours over the entire map at any selected grain size. A new map for a different grain size is thus achieved by a very simple five-step procedure:

(1) Use Equation 8 to determine the lower limiting grain size for Harper–Dorn creep.

(2) Determine the intercept on the σ/G axis from Equation 6 if $\dot{\epsilon}_{NH} > \dot{\epsilon}_{HD}$ or from Equation 7 if $\dot{\epsilon}_{NH} < \dot{\epsilon}_{HD}$.

(3) Determine the intercept on the T_m/T axis from Equation 9 if $\dot{\epsilon}_{NH} > \dot{\epsilon}_{HD}$ or from Equation 11 if $\dot{\epsilon}_{NH} < \dot{\epsilon}_{HD}$.

(4) Draw the field boundaries parallel to those already calculated for the initial grain size.

(5) Place the strain rate contours at the same positions within the climb field, and complete the contours using Equation 13.

6. Construction of an Ashby map for σ/G versus T/T_m

If required, it is possible to transpose the data from a plot of σ/G versus T_m/T to the standard form of σ/G versus T/T_m. An example is shown in Fig. 6, representing the data of Fig. 2 for aluminium with $d = 100\,\mu m$. In view of the added complexity in drawing a map of this type, it seems preferable to construct the maps in the form of σ/G versus T_m/T.

7. Discussion

The deformation mechanism maps developed in this report represent a simplified version of the Ashby map for conditions of high temperature creep ($\sigma/G \leqslant 10^{-3}$ and $T \geqslant 0.4\,T_m$). They have two significant advantages over the standard maps: (1) they are very easy to construct without the use of a computer, and (2) there is a simple procedure for constructing several maps for the same material at different grain sizes. Furthermore, the construction procedure permits the presentation of the

*A comparison of Figs. 4 and 5 reveals a slight difference in the position of the two strain rate contours within the Harper–Dorn field. This difference arises because Fig. 4 relates to a grain size of 370 μm, when Harper–Dorn and Nabarro–Herring creep both contribute equally to the strain rate. At larger grain sizes, when $\dot{\epsilon}_{NH}$ is significantly lower than $\dot{\epsilon}_{HD}$, the strain rate contours in the Harper–Dorn field are independent of the value of d.

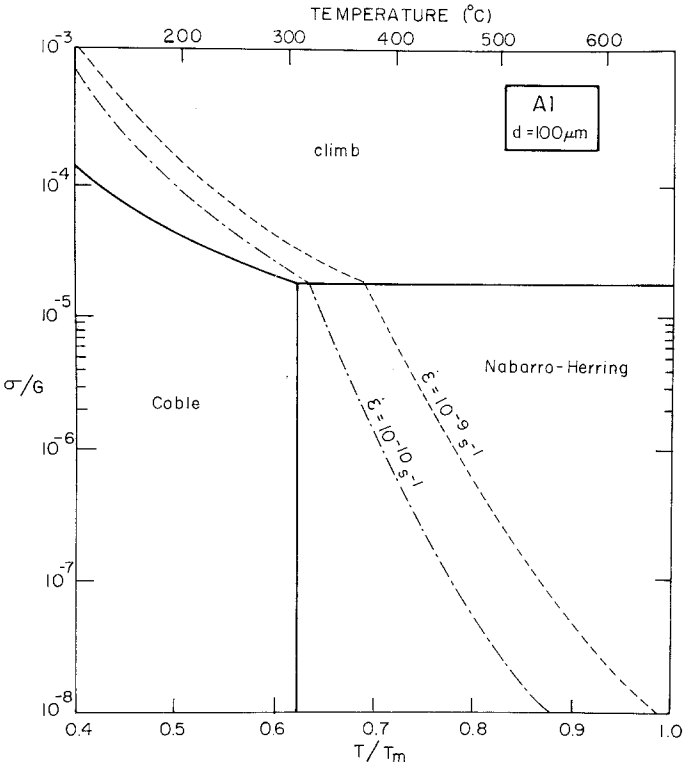

Figure 6 The data of Fig. 2 transposed to an Ashby-type deformation mechanism map for conditions of high temperature creep ($\sigma/G \leqslant 10^{-3}$ and $T \geqslant 0.4\,T_m$).

maps either in the simple format of σ/G versus T_m/T or, if required, by transposing to the more usual form of σ/G versus T/T_m.

As indicated in earlier reports [38–41], the accuracy of all maps is necessarily limited by the accuracy of the constitutive relationships used in their construction. This limitation is of relatively minor importance for pure aluminium, but may be important in other materials where there is less good experimental data to establish the various terms in the constitutive equations. A detailed discussion of the use of deformation mechanism maps in the prediction of creep behaviour was presented earlier [46].

8. Summary and conclusions

(1) It is demonstrated that the Ashby-type deformation mechanism map may be considerably simplified by plotting in the form of normalized stress, σ/G, versus the reciprocal of the homologous temperature, T_m/T. In this form, the field boundaries appear as straight lines, and the constant strain rate contours may be approximated as straight lines.

(2) Representative maps are presented for pure aluminium under conditions of high temperature creep ($\sigma/G \leqslant 10^{-3}$ and $T \geqslant 0.4\,T_m$).

(3) A simple procedure is outlined for constructing several maps for the same material at different grain sizes.

(4) If required, these maps may be transposed to the standard form of σ/G versus T/T_m.

Acknowledgement

This work was supported by the United States Energy Research and Development Administration under Contract EY-76-S-03-0113 PA-26.

References

1. J. WEERTMAN and J. R. WEERTMAN, "Physical Metallurgy", edited by R. W. Cahn (North-Holland, Amsterdam, 1965) p. 793.
2. J. WEERTMAN, *Trans. Amer. Soc. Metals* **61** (1968) 681.
3. M. F. ASHBY, *Acta Met.* **20** (1972) 887.
4. R. L. STOCKER and M. F. ASHBY, *Rev. Geophys. Space Phys.* **11** (1973) 391.
5. M. F. ASHBY, "The Microstructure and Design of Alloys", Vol. 2 (The Institute of Metals and The Iron and Steel Institute, London, 1973) p. 8.
6. J. T. A. ROBERTS and J. G. VOGLEWEDE, *J. Amer. Ceram. Soc.* **56** (1973) 472.
7. P. A. URICK and M. R. NOTIS, *ibid* **56** (1973) 570.
8. J. H. GITTUS, *Phil. Mag.* **30** (1974) 751.
9. M. R. NOTIS, *J. Amer. Ceram. Soc.* **57** (1974) 271.
10. *Idem, Powder Met. Int.* **6** (1974) 82.
11. M. F. ASHBY and H. J. FROST, "Constitutive

Equations in Plasticity", edited by A. S. Argon (MIT Press, Cambridge, Mass., 1975) p. 117.
12. H. J. FROST and M. F. ASHBY, "Rate Processes in Plastic Deformation of Materials", edited by J. C. M. Li and A. K. Mukherjee (American Society for Metals, Metals Park, Ohio, 1975) p. 70.
13. M. F. ASHBY and R. RAJ, "The Mechanics and Physics of Fracture" (The Metals Society, London, 1975) p. 148.
14. M. R. NOTIS, "Deformation of Ceramic Materials", edited by R. C. Bradt and R. E. Tressler (Plenum Press, New York, 1975) p. 1.
15. A. SAMUELSSON and A. THOLEN, "Grain Boundaries in Engineering Materials", edited by J. L. Walter, J. H. Westbrook and D. A. Woodford (Claitor's Publishing Division, Baton Rouge, 1975) p. 107.
16. F. W. CROSSMAN and M. F. ASHBY, *Acta Met.* **23** (1975) 425.
17. M. R. NOTIS, R. H. SMOAK and V. KRISHNAMACHARI, *Mater. Sci. Res.* **10** (1975) 493.
18. D. B. KNORR and M. R. NOTIS, *J. Nuclear Mater.* **56** (1975) 18.
19. M. F. ASHBY, *J. Geol. Soc.* **132** (1976) 558.
20. S. WHITE, *Phil. Trans. Roy. Soc. A* **283** (1976) 69.
21. M. S. PATERSON, *ibid* **283** (1976) 163.
22. E. H. RUTTER, *ibid* **283** (1976) 203.
23. R. K. BHARGAVA, J. MOTEFF and R. W. SWINDEMAN, *Met. Trans.* **7A** (1976) 879.
24. B. K. ATKINSON, *Earth and Planetary Sci. Lett.* **29** (1976) 210.
25. L. C. A. SAMUELSSON, K. N. MELTON and J. W. EDINGTON, *Acta Met.* **24** (1976) 1017.
26. R. N. SINGH, *J. Nuclear Mater.* **64** (1977) 167.
27. V. KRISHNAMACHARI and M. R. NOTIS, *Mater. Sci. Eng.* **27** (1977) 83.
28. R. A. VERRALL, R. J. FIELDS and M. F. ASHBY, *J. Amer. Ceram. Soc.* **60** (1977) 211.
29. B. ILSCHNER, "Hochtemperatur-Plastizität", Reine und angewandte Metallkunde in Einzeldarstellungen, Vol. 23 (Springer–Verlag, Berlin, 1973) p. 258.
30. J. GITTUS, "Creep, Viscoelasticity and Creep Fracture in Solids" (John Wiley, New York, 1975) p. 274.
31. A. G. EVANS and T. G. LANGDON, *Prog. Mater. Sci.* **21** (1976) 171.
32. A. G. GUY, "Essentials of Materials Science" (McGraw–Hill, New York, 1976) p. 324.
33. R. W. HERTZBERG, "Deformation and Fracture Mechanics of Engineering Materials" (John Wiley, New York, 1976) p. 156.
34. W. D. KINGERY, H. K. BOWEN and D. R. UHLMANN, "Introduction to Ceramics", 2nd edition (John Wiley, New York, 1976) p. 745.
35. J.-P. POIRIER, "Plasticité à Haute Température des Solides Cristallins" (Eyrolles, Paris, 1976) p. 156.
36. A. NICOLAS and J.-P. POIRIER, "Crystalline Plasticity and Solid State Flow in Metamorphic Rocks" (John Wiley, London, 1976) p. 403.
37. S. M. COPLEY and J. C. WILLIAMS, "Alloy and Microstructural Design", edited by J. K. Tien and G. S. Ansell (Academic Press, New York, 1976) p. 3.
38. F. A. MOHAMED and T. G. LANGDON, *Met. Trans.* **5** (1974) 2339.
39. T. G. LANGDON and F. A. MOHAMED, *J. Mater. Sci.* **11** (1976) 317.
40. *Idem, Mater. Sci. Eng.* **32** (1978) 103.
41. *Idem, J. Mater. Sci.* **13** (1978) 473.
42. F. R. N. NABARRO, "Report of a Conference on Strength of Solids" (The Physical Society, London, 1948) p. 75.
43. C. HERRING, *J. Appl. Phys.* **21** (1950) 437.
44. R. L. COBLE, *ibid* **34** (1963) 1679.
45. J. HARPER and J. E. DORN, *Acta Met.* **5** (1957) 654.
46. F. A. MOHAMED and T. G. LANGDON, *J. Eng. Mater. Tech.* **98** (1976) 125.

Received 12 May and accepted 16 September 1977.